Electrochimica Acta 78 (2012) 236–243

Contents lists available at SciVerse ScienceDirect

Electrochimica Acta

journal homepage: www.elsevier.com/locate/electacta

Hydrothermal crystallization and modification of surface hydroxyl groups of anodized TiO_2 nanotube-arrays for more efficient photoenergy conversion

Yu-Yen Kuo [a], Tze-Huei Li [a], Jing-Neng Yao [a], Chiung-Yuan Lin [a], Chao-Hsin Chien [a,b,*]

[a] Department of Electronics Engineering, National Chiao Tung University, 1001 Tahsueh Road, Hsinchu 30010, Taiwan
[b] National Nano Device Laboratories, 1 Prosperity Road I, Hsinchu 30050, Taiwan

ARTICLE INFO

Article history:
Received 20 February 2012
Received in revised form 15 April 2012
Accepted 29 May 2012
Available online 18 June 2012

Keywords:
TiO_2 nanotube
Hydrothermal
Crystallization
Dye-sensitized solar cells
Hydroxyl group

ABSTRACT

This paper describes a crystallization method for anodized TiO_2 nanotube-array using a hydrothermal process. Pre-sintered TiO_2 nanotube-array could further crystallize without experiencing a collapse of the nanotubes under the hydrothermal environment. Applying the hydrothermal crystallization method, the transition of surface bonds of nanotube from Ti–O to Ti–OH/Ti–OH_2 can be controlled by acidic hydrothermal pH levels. Dissolution and structural transformation of nanotubes was easily induced if the hydrothermal environment became basic. These effects depicted great influence on the anchoring of carboxylate groups on the surface of TiO_2 nanotubes and affected the performance of the dye-sensitized solar cell utilizing the hydrothermally crystallized TiO_2 nanotubes as the photoelectrode. The photoenergy conversion efficiency increased from 6.40% for thermally annealed nanotubes to 7.13% for hydrothermally crystallized ones under illumination of 100 mW cm^{-2}.

1. Introduction

TiO_2 nanotubes have been widely researched in recent years for many advanced applications in photocatalytic functions, sensing technology, solar cells and photoelectrolysis [1–4]. Various methods have been proposed to prepare the TiO_2 nanotubes including template assisted deposition, the sol–gel process, the hydrothermal method and anodic oxidation [5–8]. Usually, synthetic methods, such as the sol–gel or hydrothermal method, result in randomly oriented nanotubes, while deposition with a template or anodic oxidation can fabricate one dimensionally well aligned nanotube-arrays. For anodic oxidation, the geometrical properties, such as pore diameter and the tube length of the anodized nanotubes can be easily controlled by the electrochemical conditions [9,10]. Because of the advantages of the highly ordered structure, the high surface-to-volume ratio and the ease of fabrication, there has been a lot of research focused on the photovoltaic application of anodized TiO_2 nanotubes [10–15].

However, the as-anodized TiO_2 nanotubes are amorphous. It is obviously necessary to improve the crystallinty of TiO_2 nanotubes and, among the available techniques, thermal annealing is the most commonly used method for nanotube crystallization. After being subjected to 450–500 °C thermal annealing, the nanotubes will be in pure anatase phase, which is favorable in applications of catalytic and photo energy harvesting [4,16,17]. After thermal annealing, nanotubes are in polycrystalline form with a crystallite size of 20–30 nm. To further enhance the crystallinity, Yu et al. have examined the influences on the nature of crystallization of the anodized nanotubes by hydrothermal and vapor thermal methods [18]. They have found that the surface properties and photocatalytic activities of the TiO_2 nanotubes are dependent on the method used for crystallization. Both techniques could substantially increase the TiO_2 crystallite sizes [19–21]. Nevertheless, severe collapse of the nanotubes would be simultaneously induced during the hydrothermal process, thus making hydrothermal methods an inapplicable method for improving the crystallinity of nanotubes.

Herein, we found the hydrothermally induced collapse problem can be prevented by employing a pre-sintering technique. The crystallinity of the hydrothermally crystallized nanotubes was better than those crystallized by thermal annealing. Besides, great influence of the hydrothermal pH level on the resulting surface hydroxyl groups and on the structure of the hydrothermally crystallized nanotubes were identified. Different bonding types on the surface did affect the adsorption of carboxylate groups of bipyridyl dyes on the nanotube and greatly impact the photovoltaic performance of the fabricated solar cells.

2. Experimental

2.1. Preparation of the free-standing nanotube-array

To fabricate TiO_2 nanotube-arrays, anodization of Ti foil (0.25 mm, Alfa Aesar) was carried out at 50 V, 40 °C in solution

* Corresponding author at: Department of Electronics Engineering, National Chiao Tung University, 1001 Ta-Hsueh Road, Hsinchu 30010, Taiwan.
Tel.: +886 3 5712121x54252; fax: +886 3 5724361.
E-mail address: chchien@faculty.nctu.edu.tw (C.-H. Chien).

0013-4686/$ – see front matter © 2012 Elsevier Ltd. All rights reserved.
http://dx.doi.org/10.1016/j.electacta.2012.05.157

containing 0.3 wt% NH_4F and 2 vol% H_2O in ethylene glycol with Pt serving as the counter electrode. The bias was provided by a DC power supply, and the temperature of the overall reaction was controlled by a temperature-static tank. Before the anodization, the Ti foil was first cleaned by sonication in de-ionized water and in isopropanol, and a preliminary anodizaiton of the cleaned Ti foil was firstly applied for 30 min at 10 °C. After the first anodization, the firstly anodized TiO_2 layer was removed by sonication in water so that the surface of the Ti foil was textured to enhance the ordering of the TiO_2 nanotubes formed afterward. Then, the TiO_2 nanotube-array was fabricated by anodization for 1–2 h at 40 °C.

After the anodization, the TiO_2 nanotube-array was sintered at 400 °C for 1 h under atmospheric ambient. Next, the pre-sintered sample of TiO_2 nanotubes was set in a 23 ml autoclave, and 10–14 ml solution was filled into the Teflon aligner of the autoclave. The autoclave was heated to 240 °C in an oven using a heating rate of 6 °C min^{-1} for the hydrothermal reaction. After the hydrothermal reaction process proceeded for 2 h, the autoclave was allowed to cool to room temperature naturally. Then, the sample was moved out and the surface of the nanotubes was cleaned using CF_4/CHF_3 plasma to remove disoriented nanotubes. The sample was finally anodized again at 50 V for 30 min to cause detachment of the nanotube-array. Next, the third anodized layer was dissolved in 2 M HCl solution, and the TiO_2 nanotube-array was separated from the Ti substrate to be a free standing membrane.

2.2. Fabrication and measurement of solar cells

The detached nanotube membrane was bonded to fluorine doped tin oxide (FTO, 12 Ω □$^{-1}$) glass. The sol of titanium isopropoxide in acetic acid mixed with polyethylene glycol was used to bond the closed ends of the TiO_2 nanotubes to the FTO glass. The nanotube-array bonded on FTO was annealed at 400 °C 1 h for sintering of the bonding sol and the removal of residual solution. The peripheral edges of the nanotube region were cleaned by tape to remove additional TiO_2 particles formed by the sol. The nanotube-array was then immersed into 3×10^{-4} M N3 (cis-di(thiocyanato)-bis(2,2′-bipyridyl-4,4′-dicarboxylic acid)-ruthenium(II)) or N719 (bis(tetrabutylammonium)[cis-di(thiocyanato)-bis(2,2′-bipyridul-4-carboxylate-4′-carboxylic acid)-ruthenium(II)]) solution for 12 h. To measure the amount of the dye adsorbed by the nanotubes, the dye was desorbed into 5 mM KOH aqueous solution, and the concentration of the desorbed solution was measured by UV–Visible spectroscopy.

To fabricate the solar cell, the dye loaded nanotube-array was used as one electrode, and Pt sputtered FTO was used as the counter electrode. The two electrodes were spaced by a 60 μm thermoplastic film, and an electrolyte containing 0.05 M I_2, 0.1 M LiI, 0.5 M 4-tert-butylpyridine and 0.6 M 1-propyl-3-methylimidazolium in 3-methoxypropionitrile, was filled into the space. The photovoltaic characteristic of the fabricated cell was measured by an electrical sourcemeter (Keithley 2400) with the cell illuminated by a solar simulator (Oriel 96000) with a global AM 1.5 filter. The illumination power density was modified to be 100 mW cm^{-2} by a power meter (840-C, Newport).

The internal charge recombination rates of the fabricated cells were measured by electrical impedance spectroscopy (EIS) using a potentiostat (EG&G 273A) equipped with a frequency response analyzer. DC bias ranged from 0.5 V to 0.7 V with AC signal of 5 mV amplitude was applied and the recorded frequency range was 10^5 to 10^{-2} s^{-1}.

2.3. Characterizations of nanotubes

The prepared free-standing nanotube-array was bonded onto the glass substrate in order to characterize the crystalline properties by measuring the grazing incidence X-ray diffraction (GIXRD) using a PANalytical X'Pert Pro diffractometer with Cu Kα radiation. In order to analyze the surface bonding modes of the dye molecules on the surface of the hydrothermally treated nanotubes, the nanotube-array was bonded to the intrinsic silicon wafer for measurement of the Fourier transformed infrared spectroscopy (FTIR) using a QS-300 FT-IR spectrometer (BIO-RAD). The measurement of X-ray photoelectron spectroscopy (XPS) was performed using a VG Scientific Microlab 310F system with an Mg Kα source, and the XPS binding energies were calibrated using an additionally deposited Pt pad on the substrate.

2.4. The first-principles calculations of the nanotubes

The first-principles calculations of the anatase nanotubes are performed in the framework of density functional theory (DFT) with the Perdew–Burke–Ernzerhof (PBE) exchange correlation functional and the projector augmented wave (PAW) basis, as implemented in the Vienna Ab-initio Simulation Package (VASP). The plane-wave energy cutoff is taken to be 400 eV. The anatase nanotubes follow the same crystal geometries proposed by Bandura and Evarestov [22]. One first takes an infinitely long belt of a single anatase sheet with its length and width in the (1 0 1) and (0 1 0) directions, respectively, and then the sheet is rolled along (0 1 0) to form a tube. This tube structure is then relaxed by DFT calculations.

3. Results and discussion

3.1. Effects of pre-sintering temperature and hydrothermal solution volume

To sustain the high pressure environment in the hydrothermal process, the as-anodized TiO_2 nanotubes have to be pre-sintered. First, we tested different pre-sintering temperature followed by a hydrothermal treatment at 240 °C in water. With pre-sintering temperature below 350 °C, most of the TiO_2 nanotubes were destroyed during the hydrothermal process. This caused a 70% shortening of tube length, and an additional nanoparticle-like structure was formed on the sidewall of remaining nanotubes. The collapse of the anodized nanotubes after hydrothermal treatment was found to be avoidable when the pre-sintering temperature was raised to 400 °C. The pre-sintered nanotubes were observed to maintain their tubular structure even after the hydrothermal process reached a temperature of 240 °C, which was higher than the reported hydrothermally induced collapse temperature of 180 °C [18].

Fig. 1 shows the XRD results of the pre-sintered nanotubes before and after the hydrothermal process of various conditions. A pure anatase phase was identified for the nanotubes after pre-sintering and hydrothermal treatment. Fig. 1a depicts the comparison of XRD of nanotubes of different pre-sintering temperature followed by the same hydrothermal condition in 10 ml water. The enhancement of crystallinity properties was clearly observed when comparing the (1 0 1) X-ray diffraction intensities of the 400 °C pre-sintered nanotubes before and after the hydrothermal process. Even lowering the pre-sintering temperature to 350 °C, followed by a hydrothermal treatment, demonstrates nanotubes with higher crystallinity properties than the 400 °C sintered sample. When the pre-sintering temperature was over 450 °C, later hydrothermal treatment in 10 ml water seemed insufficient to induce further crystallization of the nanotubes. On the other hand, Fig. 1b shows a comparison of XRD peaks of nanotubes that were pre-sintered at the same 400 °C with varying amounts of water used in the hydrothermal process. The data show a strong dependence of the

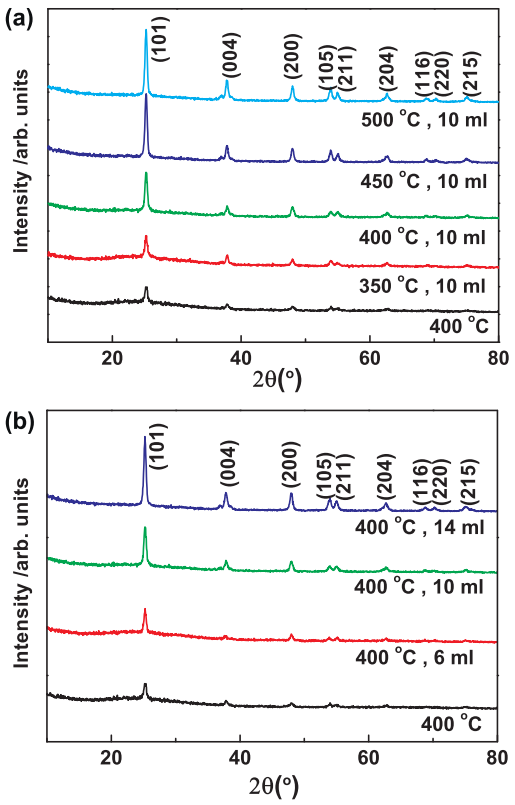

Fig. 1. XRD results of the hydrothermally crystallized nanotubes (a) with different pre-sintering temperatures and (b) with different amounts of water for the hydrothermal treatment. The anatase peaks are labeled.

crystallinity of the nanotubes on the amount of water, which is due to the rise in reaction pressure in the autoclave as the water volume increased. The crystallinity of the 240 °C hydrothermally crystallized nanotubes in 14 ml water was found to be 7% higher than that of 500 °C annealed nanotubes.

The photovoltaic characteristics of the dye-sensitized solar cells made by nanotubes fabricated with different pre-sintering temperatures and with different water volumes in the hydrothermal process are summarized in Table 1. The nanotubes were prepared by anodization at 50 V for 1 h, after which the tube length was approximately 12 μm. Solar cells using 10 ml water hydrothermally treated nanotubes with higher pre-sintering have shown better performance. This should directly result from the higher crystallinity of the nanotube pre-sintered at a higher temperature. On the other hand, the solar cells with nanotubes treated with larger amounts of water showed a better performance because of the further effects of enhanced crystallinity as well. Additionally, the adsorbed amounts of both N3 and N719 dye were noticed to be influenced by the hydrothermal conditions. Thus, the photocurrent density and the energy conversion efficiency of the cell with a lower pre-sintering temperature (400 °C) but hydrothermally treated in a larger water volume (14 ml) were higher than those of the cell pre-sintered at 500 °C but treated in 10 ml water.

3.2. Influences on nanotube morphology of hydrothermal pH

In order to elucidate the influences of the hydrothermal treatment on the surface characteristics of TiO_2 nanotubes, the hydrothermal treatment was implemented in a solution of different pH levels. The FESEM images of the nanotubes hydrothermally treated in pH1, pH3 diluted nitric acid solutions, de-ionized water, pH 10 and pH 12 potassium hydroxide aqueous solutions are shown in Fig. 2a–e. The images show that there is no apparent structural transformation of the nanotubes after hydrothermal treatment in an acidic environment of pH 1, pH 3 to pH 7; however, small particles began to arise for less basic pH 10, and the nanotubes were observed to be totally destroyed when they were treated in concentric basic conditions with pH levels higher than 12.

The destruction of the pre-sintered nanotubes under concentric basic conditions was hypothesized to arise from the induced stress of the anions (OH^-) adsorbed on the surface of the nanotubes during the hydrothermal process. We examined the DFT calculated nanotubes of different surface conditions. To simulate the nanotubes being treated with “less basic” or “highly basic” solutions, we placed hydroxyl ions on both the inner and outer surfaces of a nanotube, under half and full coverages. The relaxed structures of the different coverages are shown in Fig. 3. As can be identified

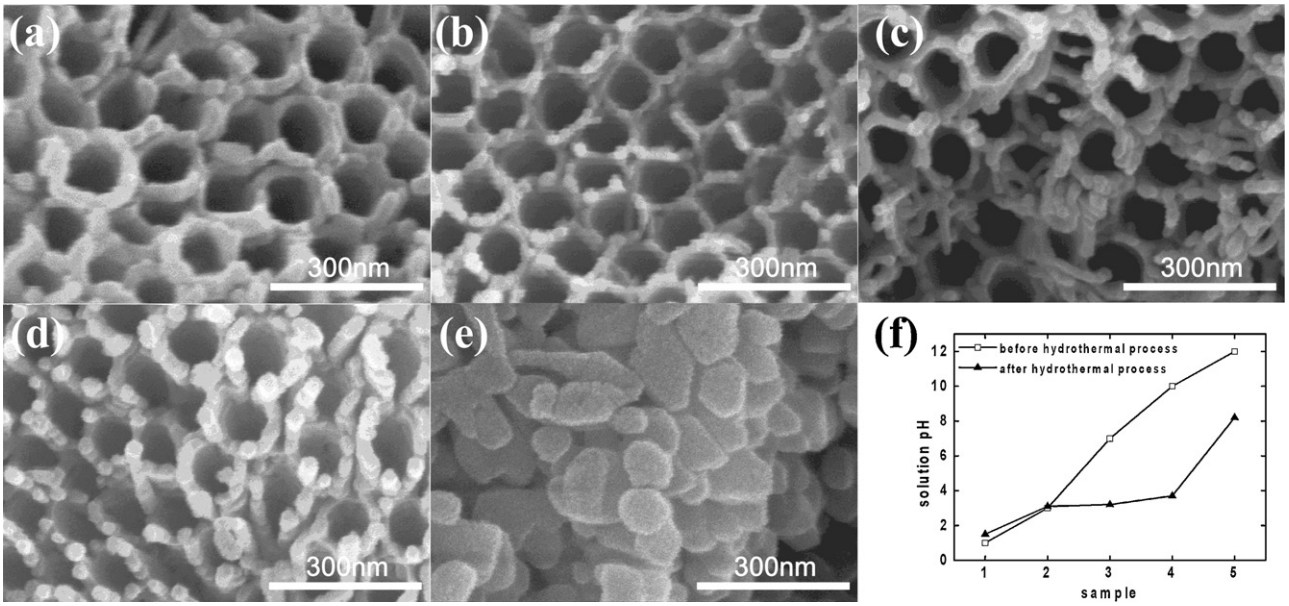

Fig. 2. FESEM images of nanotubes hydrothermally treated in HNO_3 of (a) pH 1, (b) pH 3, in (c) water and in KOH of (d) pH 10, (e) pH 12, and (f) the solution pH before/after the hydrothermal process.

Table 1
The photovoltaic properties of the dye-sensitized solar cells using 240 °C hydrothermally crystallized TiO_2 nanotubes of different pre-sintering temperature and water volume.

Pre-sintering temperature [°C]	Hydrothermal water volume [ml]	Dye	Dye load [10^{-8} mol cm^{-2}]		V_{oc} [V]	Fill factor	Power conversion efficiency [%]
400	10	N3	6.59	5.67	0.69	0.69	2.70
400	10	N719	6.51	4.52	0.74	0.72	2.41
500	10	N3	9.61	7.10	0.75	0.67	3.65
500	10	N719	8.20	6.11	0.75	0.64	2.92
400	14	N3	14.44	9.40	0.74	0.66	4.56
400	14	N719	13.96	8.63	0.75	0.65	4.19

in the figures, there are significant rearrangements of the atomic positions and chemical bonds after the adsorption of the hydroxyl groups. Each pair of nearest inner and outer hydroxyl ions stretched the half-coverage tube along the normal direction of the tube wall, causing a breaking Ti–O bond. The full-coverage tube was even more complex, and had the hydroxyl ions undergo recombination to form water molecules and ligands. We quantified the geometry change of the hydroxyl-covered anatase nanotubes by an O–Ti–O bond angle θ as in the figures. The θ angle increased from 83.8° of a clean tube to 94.0° of less basic tube, and finally reached 104.4° for the highly basic one. The O–Ti–O bond angle highly depended on the coverage density of the hydroxyl groups.

Also, Fig. 2f shows a change of pH value in the solutions after the hydrothermal reaction. Interestingly, we noticed that pH levels less than 3 slightly increased after the hydrothermal process whereas those pHs greater than 3 dropped dramatically. This tendency indicated a decreased H+ concentration in the solutions of pH less than 3 and an increased H+ concentration in the solutions of water under basic conditions. As a result, we suggested that acidic and basic solutions induce an opposite surface polarity on the hydrothermally treated nanotubes.

3.3. Influences on crystalline and surface bonding properties of hydrothermal pH

Fig. 4 is the XRD spectra of the nanotubes hydrothermally treated in solutions of different pH levels. The influence of the anion or cation in the acidic hydrothermal environment on the crystallinity and the crystallite size of the nanotubes are not appreciable; both the full width at half maximum (FWHM) and the peak intensities showed similar values. In contrast, a decrease on FWHM of the destroyed nanotube of basic pH could be identified, which meant a larger crystallite size of 24 nm was produced; this could be also be judged from the FESEM images of the collapsed nanotubes as well. Additional aggregation of the TiO_2 particles on the sidewall of the destroyed nanotube could more easily happen in the hydrothermal process and therefore cause a further increased crystallite size [18].

After applying these hydrothermally treated nanotubes to fabricate the solar cells, we found there was a significant dependence of the photovoltaic characteristics of the solar cells on the pH of the hydrothermal solution. Table 2 summarizes the photovoltaic parameters of these cells; the nanotubes were all fabricated at 50 V, 40 °C for 2 h, with a length of 18 μm. The best performing cells were nanotubes treated in water. The photocurrent density and power conversion efficiency decreased markedly when the nanotubes were treated in a more acidic or more basic environment. This strong dependence of the photocurrent on hydrothermal pH value result was noticed to be from the greatly varying dye loads in the nanotubes treated in the solutions of different pH values. The measured amount of the dye adsorbed showed a peak on the nanotube treated in water and decreased once the hydrothermal environment became more acidic or more basic; similar dependencies were clearly observed in both the N3 dye and the N719 dye. For basic pH levels, the decrease on dye adsorption should directly result from the decreased surface area of the structurally transformed nanotubes, but for acidic pH levels, this behavior might be due to the changed surface chemistry after the hydrothermal process. On the other hand, in contrast to the decreased photocurrent density for both acidic and basic conditions, the open-circuit voltage of the cells showed an opposite shift. A decreased V_{oc} for the acidic condition and an increased V_{oc} for the basic condition could be identified from the table. We thus hypothesized this result could directly result from a change on surface dipoles induced during the hydrothermal process of different pH conditions as discussed previously. A similar dependence was also observed on the solar cell of nanotubes treated at pH12 even though a destroyed structure was identified.

Fig. 5a shows the FTIR spectra of the nanotubes undergoing hydrothermal treatment at different pH levels. By comparing the spectrum of nanotubes adsorbed with N719 to that of the bare nanotubes without dye, the presence of the carboxylic acid and carboxylate groups of N719 was identified. As noted in Fig. 5b, in

Table 2
The photovoltaic properties of dye-sensitized solar cells using 18 μm TiO_2 nanotubes treated by different hydrothermal pH levels.

Hydrothermal pH	Dye	Dye load [10^{-8} mol cm^{-2}]	J_{sc} [mA cm^{-2}]	V_{oc} [V]	Fill factor	Power conversion efficiency [%]
pH 1	N3	13.24	5.99	0.71	0.62	2.63
pH 1	N719	10.26	4.43	0.70	0.70	2.16
pH 2	N3	17.47	7.27	0.70	0.62	3.17
pH 2	N719	12.87	6.49	0.70	0.55	2.48
pH 3	N3	21.46	10.49	0.68	0.70	4.99
pH 3	N719	15.04	8.27	0.69	0.69	3.92
Water	N3	26.84	11.59	0.71	0.61	5.02
Water	N719	20.23	9.48	0.72	0.68	4.61
pH 10	N3	20.71	7.61	0.74	0.68	3.84
pH 10	N719	14.58	7.23	0.73	0.72	3.79
pH 11	N3	17.35	6.90	0.74	0.69	3.51
pH 11	N719	11.05	6.09	0.72	0.69	3.02
pH 12	N3	10.27	5.06	0.73	0.65	2.39
pH 12	N719	8.15	3.39	0.73	0.63	1.56

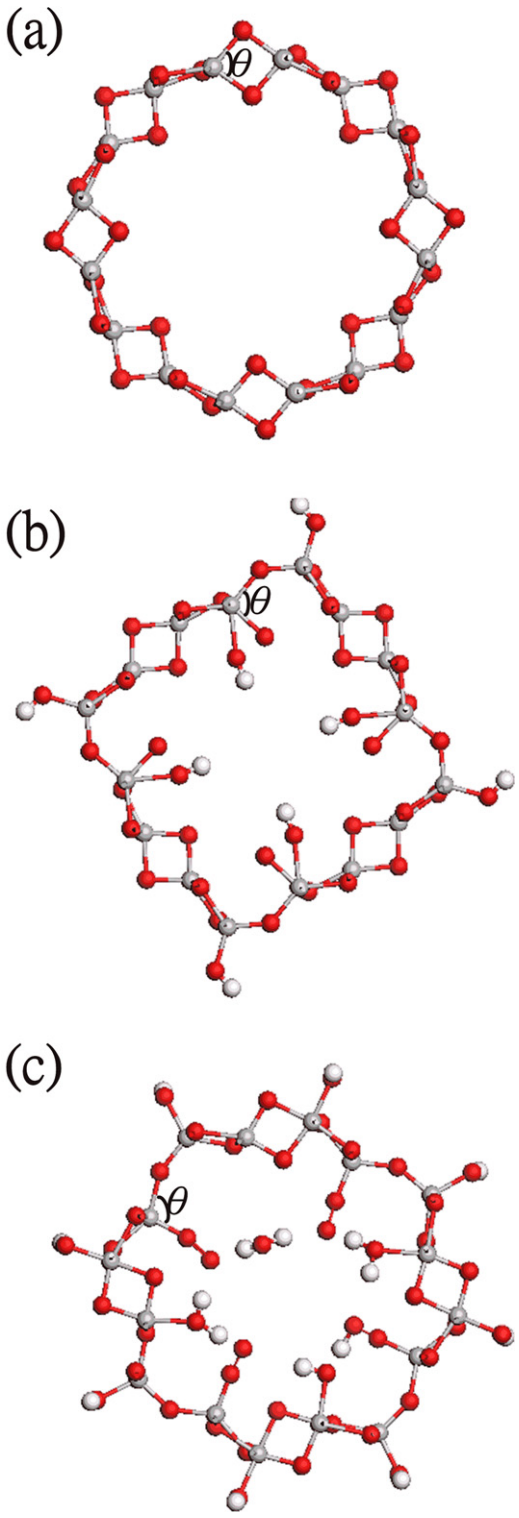

Fig. 3. The DFT calculated TiO_2 nanotubes with (a) clean surface, (b) surface half covered by hydroxyl ions, and (c) surface fully covered by hydroxyl ions.

the low wavenumber region the FTIR spectra of the N719 sensitized nanotubes treated in pH 3, water and pH 10 similarly showed the carbonyl stretch band at 1717 cm^{-1}, the carboxylate vibrations of ν(COO-sym and COO-asym) at 1601–1607 cm^{-1}, 1371–1377 cm^{-1} and ν(C=O) at 1233 cm^{-1}. The ν(C=O) at 1233 cm^{-1} shows a shift less than 5 cm^{-1} to the reported ν(C=O) of 1230 cm^{-1}; this excluded the occurrence of the ester-like linkages of the N719 when

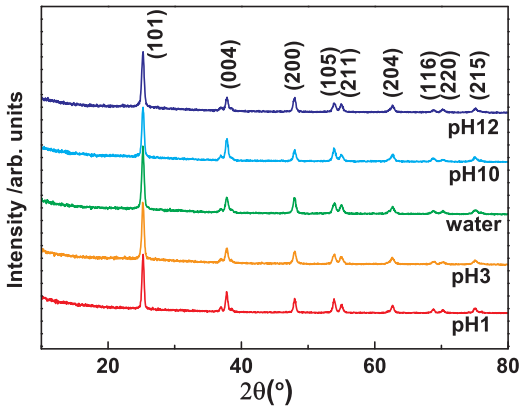

Fig. 4. XRD results of the nanotubes hydrothermally treated within solutions of different pH levels. The anatase peaks are labeled.

adsorbing onto the hydrothermally crystallized nanotubes according to Falaras's research [23]. By taking the carboxylate difference ($\Delta\nu = \nu$(COO-sym) – ν(COO-asym)), the binding mode of the N719 could be further identified [24,25]. The $\Delta\nu$ are 232 cm^{-1}, 230 cm^{-1} and 230cm^{-1} for N719 adsorbed on nanotubes treated in solution of pH 3, water and pH 11, respectively. With $\Delta\nu$ less than 235cm^{-1}, which is the $\Delta\nu$ of neat state of N719, the binding of the N719 on the nanotubes of different hydrothermal pH levels should be in the same mode of bidentate bridging.

In the high wavenumber region of the FTIR spectrum, ν(NC) of thiocyanate were found at 2098–2010 cm^{-1} for N719 adsorbed on hydrothermally treated nanotubes. The shift of the ν(NC) was found to be less than the reported shift for N719 adsorbed on TiO_2 nanoparticles, which indicated a weaker interaction between the thiocyanate of N719 and the TiO_2 nanotubes. In the high

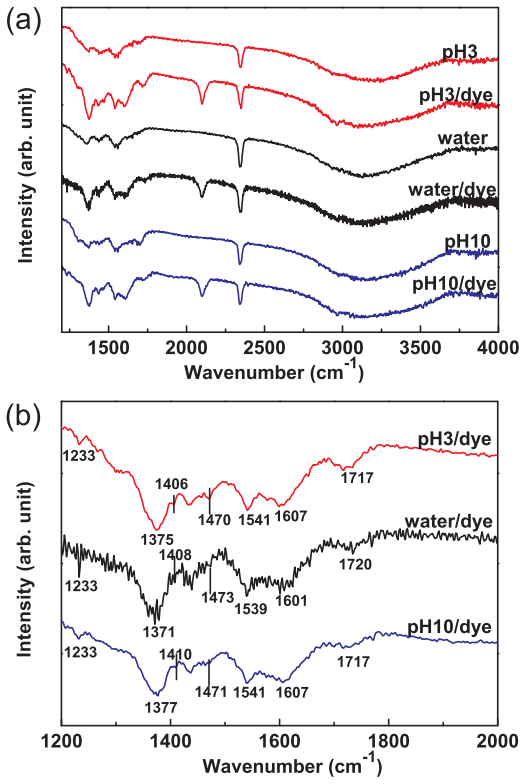

Fig. 5. (a) The FTIR spectra of the nanotubes of different hydrothermal pH conditions. (b) The low wavenumber region and the characteristic peaks for the FTIR spectroscopy of N719 adsorbed on nanotubes.

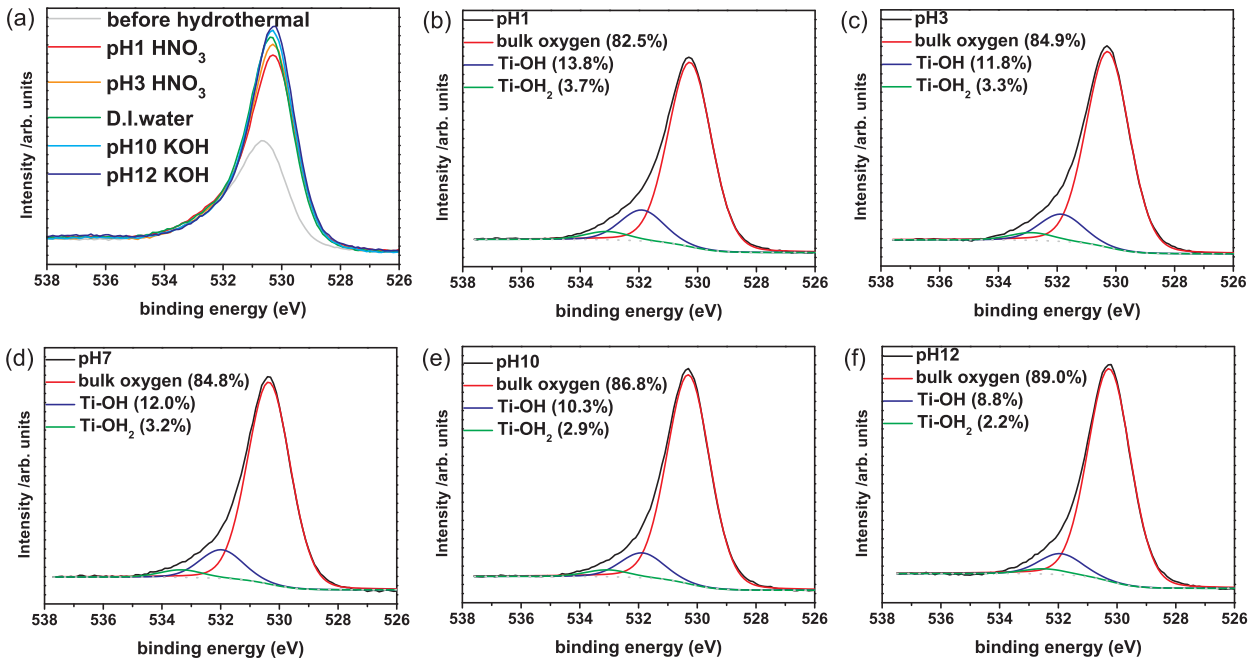

Fig. 6. O 1s XPS of (a) as prepared and hydrothermally treated TiO_2 nanotubes in different solution: (b) HNO_3, pH 1; (c) HNO_3, pH 3; (d) water; (e) KOH, pH 10; and (f) KOH, pH 12.

wavenumber region of the FTIR spectra of the nanotubes, there was a broad band at ca. 3200 cm^{-1}; this should result from the presence of hydroxyl groups, Ti–OH/Ti–OH_2, on TiO_2 surface [24,26]. Within the broad band, the occurrence of peaks at 2962–2966 cm^{-1} for N719 adsorbed nanotubes was ascribed to CH_3 of tetrabutylammonium (TBA) cations as the $\nu(CH_2)$ in TBA also found at 1470 cm^{-1} [27].

According to the FTIR results of N719 adsorbed nanotubes, the bonding mode of the dye on the surface of hydrothermally treated nanotubes in different pH levels have been known to be similarly in bidentate bridging. The influence of pH on the amount of dye adsorption might arise from the change of electronic interactions between the dye and the surface groups of nanotubes. For further insight, the XPS analyses of the hydrothermally treated nanotubes were performed. Fig. 6 shows the O 1s XPS results of the nanotubes hydrothermally treated in various acidic and basic conditions. Asymmetric broadening, which has been known to come from Ti–OH/Ti–OH_2 groups on the TiO_2 surface, toward higher binding energy of the main peak of Ti–O/bulk oxygen can be identified in the spectra [28,29]. In Fig. 6a, there was a significant increase on the bulk oxygen peak after the hydrothermal treatment. This should be caused by the improved crystallinity after the hydrothermal treatment since better crystallinity could reduce the scattering probability of excited electrons from bulk oxygens. According to

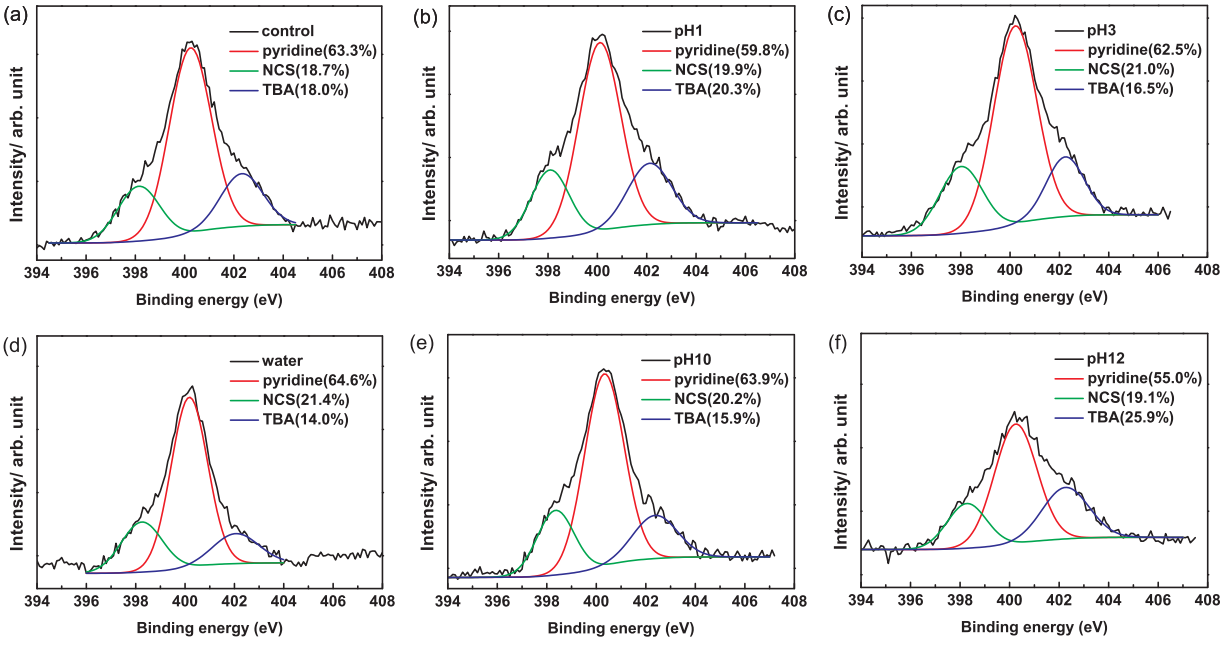

Fig. 7. N 1s XPS of N719 dye adsorbed on (a) as prepared and hydrothermally treated TiO_2 nanotubes in different solution: (b) HNO_3, pH 1; (c) HNO_3, pH 3; (d) water; (e) KOH, pH 10; and (f) KOH, pH 12.

Simmons and Beard's work, the O 1s peak can be resolved into three Gaussian peaks associating with the oxygen in the TiO_2 bulk, the oxygen of Ti–OH and the oxygen of Ti–OH_2 from low to high binding energies [28]. Based on this method, the O 1s XPS of the hydrothermally treated nanotubes were resolved as shown in Fig. 6b–f. The peaks of the bulk oxygen, the Ti–OH and the Ti–OH_2 were observed at ca. 530.3 eV, 532.2 eV and 533.3 eV respectively. By comparing the resolved components of the XPS of nanotubes with different hydrothermal pH, we found that the ratio of Ti–O/bulk oxygen gradually increased concomitant with the gradually decreased ratio of Ti–OH and Ti–OH_2 as the pH increased. This result suggested the surface oxygens or Ti–OH on TiO_2 nanotubes could react with hydrogen ions and thus lead to more Ti–OH and Ti–OH_2 in more acidic environment. On the other hand, hydrogen ions could be released via the dissociation of Ti–OH and Ti–OH_2 when the solution was in basic condition. As a result, the reason why the pH less than 3 slightly increased whereas those pHs greater than 3 dropped dramatically shown in Fig. 2f could be well explained.

Fig. 7 depicts N 1s XPS of N719 dye adsorbed on the as prepared and hydrothermally treated TiO_2 nanotubes in different solutions of varying pH levels. After dye absorption on the nanotubes, significant differences of N 1s XPS for the hydrothermally treated nanotubes were observed. According to the study of Johansson et al., the N 1s spectra of N719 can be resolved to three peaks corresponding to NCS, pyridine and TBA [30,31]. Strong dependence of the detected TBA signal on the hydrothermal pH value was observed. There were two possible sources contributing the TBA signal. One came from the non-dissociated TBA of the N719, and the other was due to the dissociated TBA cation adsorbed on the TiO_2 surface [27]. The ratio change on the detected TBA for N719-sensitized nanotube with different hydrothermal pH should be primarily caused by the dissociated TBA cation adsorbed on the TiO_2 surface. As examined before, the amount of the adsorbed dye on hydrothermally treated TiO_2 nanotube heavily decreased as the hydrothermal solution became more acidic or more basic. Therefore, there were more sites available for the dissociated TBA adsorption, which resulted into the increase on TBA portion of N 1s XPS signal. Also, it is noteworthy that the decreased dye load on nanotubes of more acidic or more basic pH should not be caused by the TBA cation since a similar dependence was also observed for N3 dye, of which TBA is lacked.

3.4. Enhancement of photoenergy conversion efficiency of hydrothermally crystallized nanotubes

Previous results showed improved energy conversion efficiency when dye-sensitized solar cells use TiO_2 photoelectrode nanotubes hydrothermally crystallized in water under high pressure. Accordingly, we further examined the dye solar cells of thermally annealed nanotubes with hydrothermal treatment in increased amount of water. As Fig. 8a shows, when TiO_2 nanotubes were thermally annealed at 480 °C for 3 h, the fabricated solar cell exhibited 6.40% energy conversion efficiency under illumination of 100 mW cm^{-2}. After hydrothermal treatment at 240 °C in 15 ml or 16 ml water for 4 h, the energy conversion efficiency of the solar cell using a nanotube photoelectrode can be further improved to 7.10% and 7.13% respectively. The short-circuit current density J_{sc} increased from 13.23 mA cm^{-2} to 13.81 mA cm^{-2}, and the open-circuit voltage V_{oc} increased from 0.70 V to 0.73 V. The charge recombination rates of the cells measured by electrical impedance spectroscopy also showed differences. As Fig. 8b shows lower charge recombination rates in hydrothermally treated nanotubes compared to those of thermally annealed nanotubes at 0.5–0.7 V can be identified. This enhancement could result directly from the better crystalline properties and the transformed surface bonds of the hydrothermally treated nanotubes. As shown in Fig. 9, the TiO_2 nanotubes were

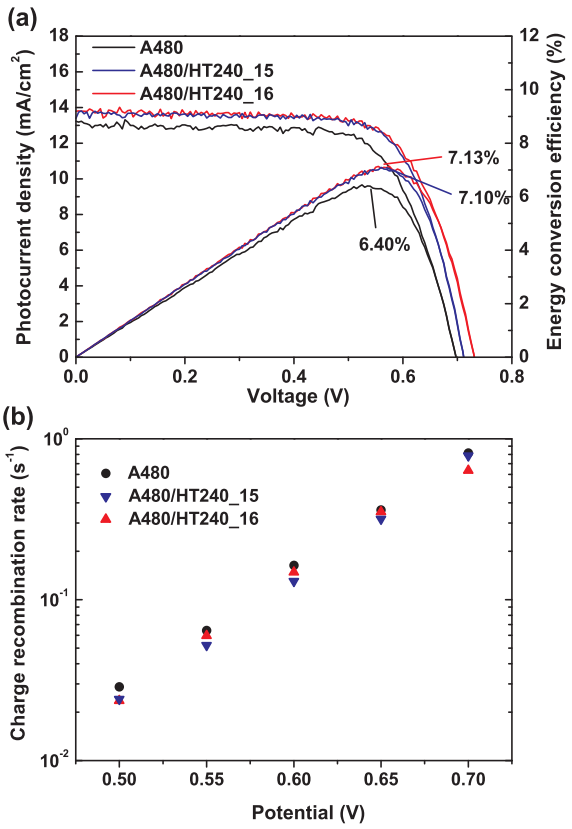

Fig. 8. (a) The photocurrent density–voltage plot and (b) the charge recombination rates of the N719-sensitized solar cell in front side illumination mode using 480 °C 3 h annealed nanotubes (A480) followed by 240 °C, 4 h hydrothermal treatment in 15 (HT240_15) or in 16 ml (HT240_16) water. The nanotubes were fabricated at 50 V for 2 h at 40 °C.

all in pure anatase phase, and there was approximately 10% difference on crystallinity of the 480 °C annealed nanotube before and after the 240 °C hydrothermal treatment.

For hydrothermal water volumes in excess of 16 ml, we observed the ends of pre-sintered nanotubes began to collapse and result in broken tubes on top of the oriented nanotube-array. Under such conditions, the hydrothermal pressure could become too high to the nanotubes. On the other hand, because higher temperature and higher pressure were also not sustainable in the autoclave, these hydrothermal conditions were not examined further.

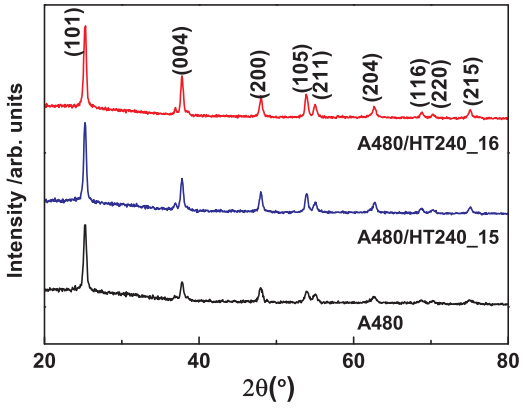

Fig. 9. XRD results of 480 °C 3 h annealed nanotubes (A480) with or without 240 °C, 4 h hydrothermal treatment in 15 (HT240_15) or in 16 ml (HT240_16) water. The nanotubes were fabricated at 50 V for 2 h at 40 °C. The anatase peaks are labeled.

4. Conclusion

The destruction of the nanotubes under the hydrothermal condition was prevented by employing a 400 °C pre-sintering process. The crystallization property and the surface bonding type of the hydrothermally treated TiO_2 nanotubes were observed to be enhanced by choosing the proper hydrothermal condition. The crystallinity of the nanotubes depended on the volume of the solution, which was related to the hydrothermal pressure. A further improved crystallinity of the hydrothermally treated TiO_2 nanotubes than that of simply thermal annealed nanotubes was identified in our experiment. The performance of the dye-sensitized solar cell using the hydrothermally treated TiO_2 nanotube as the photoelectrode was also dependent on the extent of the hydrothermally induced crystallinity properties.

We also found that the hydrothermal pH did influence the surface bonding type of the TiO_2 nanotubes. XPS studies of O 1s spectra of the hydrothermally treated nanotubes revealed that the acidic hydrothermal treatment could cause a bond transition from Ti–O and Ti–OH to Ti–OH_2 groups on the TiO_2 nanotube surface, which resulted into the heavily decreased dye loads. On the contrary, for the basic hydrothermal pH, structural destruction during the hydrothermal process still happened even after a pre-sintering process. According to DFT calculations, the dissolution of the nanotubes could be related to the stretching by adsorbed hydroxyl ions.

According to the results of our experiments, the anodized TiO_2 nanotube hydrothermally crystallized in water led to the best performance of the fabricated solar cell in contrast to cells using the nanotubes with other hydrothermal conditions. However, The TiO_2 nanotubes might be further improved if the structural transformation in the basic hydrothermal process could be prevented.

Acknowledgements

We are grateful to the National Device Laboratory for supporting XRD and XPS measurements, and acknowledge Nano Facility Center at NCTU for the use of the FESEM and the sputtering system.

References

[1] S.P. Albu, A. Ghicov, J.M. Macak, R. Hahn, P. Schmuki, Nano Lett. 7 (2007) 1286.
[2] Q. Zheng, B. Zhou, J. Bai, L. Li, Z. Jin, J. Zhang, J. Li, Y. Liu, W. Cai, X. Zhu, Adv. Mater. 20 (2008) 1044.
[3] G.K. Mor, K. Shankar, M. Paulose, O.K. Varghese, C.A. Grimes, Nano Lett. 6 (2006) 215.
[4] K. Shankar, G.K. Mor, H.E. Prakasam, S. Yoriya, M. Paulose, O.K. Varghese, C.A. Grimes, Nanotechnology 18 (2007) 065707.
[5] Thelese R.B. Foong, Y. Shen, X. Hu, A. Sellinger, Adv. Funct. Mater. 20 (2010) 1390.
[6] J.H. Jung, H. Kobayashi, J.C. Kjeld, van Bommel, S. Shinkai, T. Shimizu, Chem. Mater. 14 (2002) 1445.
[7] K.P. Yu, W.Y. Yu, M.C. Kuo, Y.C. Liou, S.H. Chien, Appl. Catal. B: Environ. 84 (2008) 112.
[8] M. Paulose, K. Shankar, S. Yoriya, H.E. Prakasam, O.K. Varghese, G.K. Mor, T.A. Latempa, A. Fitzgerald, C.A. Grimes, J. Phys. Chem. B 110 (2006) 16179.
[9] J. Park, S. Bauer, K. von der Mark, P. Schmuki, Nano Lett. 7 (2007) 1686.
[10] C.C. Chen, H.W. Chung, C.H. Chen, H.P. Lu, C.M. Lan, S.F. Chen, L. Luo, C.S. Hung, Eric W.G. Diau, J. Phys. Chem. C 112 (2008) 19151.
[11] J. Wang, Z. Lin, Chem. Mater. 22 (2010) 579.
[12] J. Lin, J. Chen, X. Chen, Electrochem. Commun. 12 (2010) 1062.
[13] Q. Chen, D. Xu, J. Phys. Chem. C 113 (2009) 6310.
[14] B.X. Lei, J.Y. Liao, R. Zhang, J. Wang, C.Y. Su, D.B. Kuang, J. Phys. Chem. C 114 (2010) 15228.
[15] Q. Zheng, H. Kang, J. Yun, J. Lee, J.H. Park, S. Baik, ACS Nano 5 (2011) 5088.
[16] K. Zhu, N.R. Neale, A. Miedaner, A.J. Frank, Nano Lett. 7 (2007) 69.
[17] Y. Sun, K. Yan, G. Wang, W. Guo, T. Ma, J. Phys. Chem. C 115 (2011) 12844.
[18] J. Yu, G. Dai, B. Cheng, J. Phys. Chem. C 114 (2010) 19378.
[19] H. Wang, Y. Liu, M. Li, H. Huang, M. Zhong, H. Shen, Appl. Phys A: Mater. Sci. Process. 97 (2009) 25.
[20] D.R. Zhang, H.G. Cha, Y.S. Kang, J. Nanosci. Nanotechnol. 11 (2011) 6007.
[21] Z. Chen, G. Zhao, H. Li, G. Han, B. Song, J. Am. Ceram. Soc. 92 (2009) 1024.
[22] A.V. Bandura, R.A. Evarestov, Surf. Sci. 603 (2009) L117.
[23] P. Falaras, Sol. Energy Mater. Sol. Cells 53 (1998) 163.
[24] K.E. Lee, M.A. Gomez, S. Elouatik, G.P. Demopoulos, Langmuir 26 (2010) 9575.
[25] K.S. Finnie, J.R. Bartlett, J.L. Woolfrey, Langmuir 14 (1998) 2744.
[26] M. Minella, M.F. Giulia, V. Maurino, C. Minero, E. Pelizzetti, S. Coluccia, G. Martra, Langmuir 26 (2010) 2521.
[27] F. Hirose, K. Kuribayashi, T. Suzuki, Y. Narita, Y. Kimura, M. Niwano, Electrochem. Solid-State Lett. 11 (2008) A109.
[28] G.W. Simmons, B.C. Beard, J. Phys. Chem. 91 (1987) 1143.
[29] K.E. Lee, M.A. Gomez, T. Regier, Y. Hu, G.P. Demopoulos, J. Phys. Chem. C 115 (2011) 5692.
[30] H. Rensmo, K. Westermark, S. Södergren, O. Kohle, P. Persson, S. Lunell, H. Siegbahn, J. Chem. Phys. 111 (1999) 2744.
[31] E.M.J. Johansson, M. Hedlund, H. Siegbahn, H. Rensmo, J. Phys. Chem. B 109 (2005) 22256.